Eng. Sci., 2022, **18**, 288–298

Engineered Science
DOI: https://dx.doi.org/10.30919/es8d672

Stability Analysis of a Lemon Bearing Operating with Non-Newtonian Lubricant Considering Slip between the Sliding Surfaces

Amar Murthy A[1] and Raghunandana K[1,*]

Abstract

With the addition of additives, lubricating fluid begins to behave non-linearly. Besides that, the emergence of ultra-high-speed machines with highly polished surfaces causes slip between the sliding surfaces, violating the no-slip boundary condition. The current novel research work looks at the performance of the bearing while considering the combined effect of the non-Newtonian and wall-slip impact of the lubricant. Furthermore, the model developed can account for the influences of slip lengths acting in orthogonal directions at the solid-fluid interface of both sliding surfaces. This innovative model produces more realistic steady-state and dynamic performance results than the classic Reynolds hypothesis. The finite difference method is employed to determine the pressure developed using the successive over-relaxation approach. The findings divulge that the occurrence of wall slip on the journal surface significantly impacts bearing performance. The journal center trajectories that determine the system's stability are estimated using non-linear transient analysis. The findings reveal that, at a power-law index of 0.75 and slip-length of 0.2, dimensionless pressure increases by 10%, resulting in higher load-carrying capacity. The flow rate is increased by 6.5%, and above all, the stability region has grown by about 19.45%.

Keywords: Lemon Bearing; Wall slip; Non-Newtonian fluid; Film thickness; Steady-state performance; Nonlinear transient analysis.
Received: 16 January 2021; Revised: 15 March 2022; Accepted: 15 March 2022.
Article type: Research article.

1. Introduction

With the advent of highly finished surfaces introduced on journal bearings to reduce friction in sliding surfaces, there exists a wall slip between the sliding surfaces and the lubricant. With the use of slip surfaces efficiently, improved, and better results can be obtained in the performance of bearings. Because of the weaker linkages between them, slide occurs on smooth sliding surfaces.[1,2] Earlier works carried out showed a reduction in friction force between the sliding surfaces, which ultimately helps increase the component's life and a drop in the consumption of energy. The tribological behavior of lubricated contacts is influenced significantly by slip surfaces.[3–5] According to studies, it is found that at a smaller eccentricity ratio and with slip on the bearing surface, the load-carrying capacity is high.[6] Many improvements in bearing properties could be achieved by optimizing the size and shape of the slippage area. An optimized slippery surface design can increase load-carrying capacity with less friction coefficient.[7] The bearings including slip and no-slip sections have better load-carrying capabilities than a traditional bearing for a given eccentricity.[8] The strategy of using a blend of texturing and slip by Susilowati *et al.*[9] showed a substantial impact on improving the bearing's performance. Rao *et al.*[10,11] studied the favorable effects and possibilities of partial slip texture on the friction coefficient, load-carrying capacity, and bearing stability using Newtonian/Non-Newtonian lubricated bearings. Qiyin *et al.* [12] showed the constructive impact of slip on sliding contacts.

In recent years, there has been much interest in using non-Newtonian fluids as lubricants in many industrial applications since they have lower friction and a larger load-carrying capacity. Incorporating the nonlinear lubricant behavior predicts the performance of the bearing to be more realistic

[1]*Department of Mechanical and Industrial Engineering, Manipal Institute of Technology, Manipal Academy of Higher Education, Manipal, Karnataka, India.*
**E-mail:* raghu.bhat@manipal.edu (Raghunandana. K)

with accurate results. Huang *et al*.[13] demonstrated that the load-carrying capacity was boosted significantly with micropolar fluid, and the friction coefficient had reduced. Compared to bearings operated using Newtonian lubricants, micropolar lubricated bearings performed superior in friction reduction and load-carrying capacity, according to Khonsari and Brewe.[14] In the case of non-Newtonian fluids, Neil *et al*.[15] numerically demonstrated that the pressure, load-bearing capacity, frictional force, and temperature rose. Compared to a purely viscous fluid, dilatant lubricants improve load-carrying performance. In an infinitely long bearing, Safar[16] examined the effects of a non-Newtonian fluid. According to his research, the load-bearing capacity and pressure increased as the power-law index grew, and the power-law index had a more substantial influence at higher eccentricity ratios. Researchers[17,18] found the power-law model to be more effective and well-suited in analyzing an elliptical bore bearing's performance characteristic with non-Newtonian liquids than the other available modes for examining non-Newtonian fluids. According to Crosby and Chetti,[19] the parameter of couple stress (non-Newtonian fluid) has a considerable impact on bearing performance when compared to Newtonian fluids, resulting in greater stability. Raghunandana and Majumdar[20] investigated the impact of non-Newtonian lubricants' stability on hydrodynamic journal bearings subjected to a continuous single-direction responsive load. Their findings show that non-Newtonian fluid influences the stability of hydrodynamic bearings, which, therefore, cannot be overlooked during the design process. Tayal *et al*.[21] investigated the effect of a non-Newtonian non-linear parameter of an additive-enhanced lubricant on the performance of an elliptical bearing. According to their observations, the apparent viscosity and friction force of two-lobed bearings dropped as the nonlinearity coefficient increased. Das and Roy[22] study revealed an increase in the stability of the multi-lobe bearing operating with a high-power law-indexed non-Newtonian fluid as a lubricant. In a study conducted by Das *et al*.[23] non-Newtonian lubricants performed significantly better than Newtonian lubricants by exhibiting higher stability thresholds. Prashant *et al*.[24] explored that the non-linearity of a non-Newtonian fluid in conjunction with wear depth and offset had a good potential in improving the bearing stability of a hybrid, worn, two-lobe journal bearing. Lin *et al*.[25] investigated and demonstrated the existence of a higher boundary of stability using non-Newtonian effects in short journal bearings using transient nonlinear analysis. Chetti *et al*.[26] studied the influence of preload and additive-enhanced lubricant of a 3-lobed bearing. Their findings demonstrated that the preload factor and non-Newtonian lubricant had a significant impact on performance attributes such as reduced friction, side leakage, and higher load-bearing capacity.

To summarise the gaps in previous research studies, it is surveyed that in earlier works, researchers focused on the influence of non-Newtonian lubricants on the performance of plain circular bearings[9-11,17] or two-lobe bearings.[13-18,21] Other studies[1-2] concentrated only on the effect of slip on plain journal bearings or two-lobe bearings.[19] Also, to add to the above gaps, Recently, Das and roy[22] investigated the influence of non-Newtonian lubricants on multilobe bearings, and Rao *et al*.[27] investigated the effect of partial slip with texturing on multilobe bearings using Newtonian fluids. Thus, to the evidence relating, no research has focused on the combined influence of non-Newtonian lubricant and wall-slip on the static and stability properties of the lemon-bearing.

Hence the present research work is novel in that it examines the combined effect of wall slip at the fluid-solid interface and the non-Newtonian impact of the lubricant on the performance of the lemon bearing. In addition to that, the created model can simultaneously address the effects of slip lengths in orthogonal directions occurring at the solid-fluid interface of both sliding surfaces. This novel model delivers more realistic steady-state and dynamic performance results than the standard Reynolds hypothesis.

The current research provides the Reynolds equation in a modification that accounts for wall slip and the non-Newtonian effect on solid-lubricant surfaces acting in the mutually perpendicular direction of the lemon bearing. The dimensionless pressure is calculated using the finite difference method (FDM) by solving the modified Reynolds equation. The steady-state performance characteristics such as load-carrying capacity, flow rate, and friction, are determined. By initially solving the equations of motion, the dimensionless mass parameter is derived for stability analysis. Non-linear transient analysis is used to determine the journal center trajectories that characterize the system's stability.

2. Methodology

2.1 Geometry of Lemon bearing

The coordinate system and the lemon-bearing configuration are demonstrated in Fig. 1. The current study focuses on the x, y, and z coordinate systems that originate at the journal center (O′). The bearing centre (O) for lower lobe (O_L) or upper lobe (O_U) centres are not concentric but at offset (d) from the geometric centre. The eccentricities of the lower and upper lobes are represented by e_L and e_U, respectively. The bearing has two clearances when the journal is concentric to the bearing: major clearance (C) and minor clearance (C_m). By

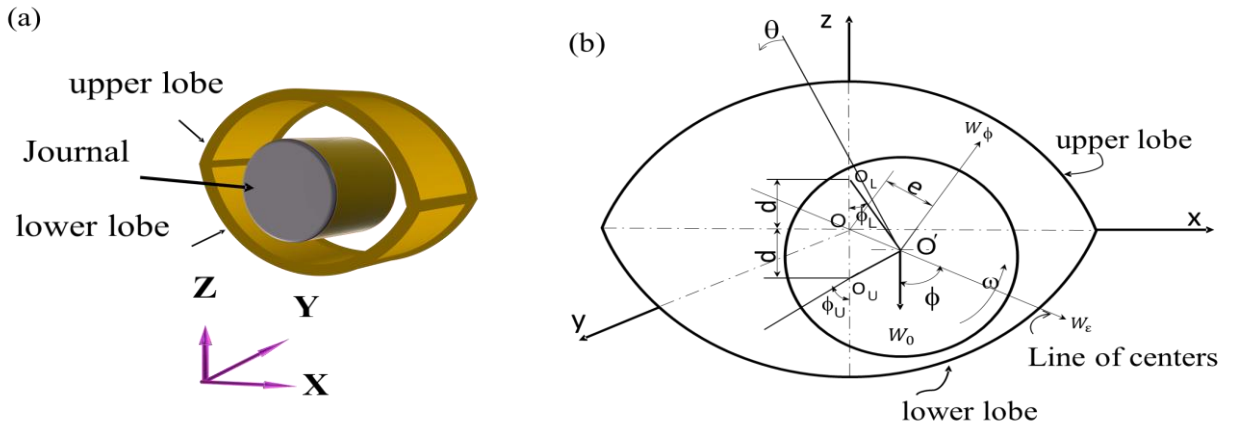

Fig. 1 Lemon bearing geometry (a) 3D view with co-ordinate system (b) Configuration of the lemon bearing system.

using trigonometric relationships, eccentricity ratios (ε_L, ε_U) and attitude angles (ϕ_L, ϕ_U) may be connected with bearing eccentricity ratio (ε), attitude angle (ϕ), and ellipticity ratio (δ) at any position of the shaft[28] as given from Eqs. (1) to (4) For the lower lobe,

$$\varepsilon_L = \sqrt{\varepsilon^2 + \delta^2 + 2\varepsilon\delta\cos\phi} \quad (1)$$

$$\phi_L = sin^{-1}\left(\frac{\varepsilon\ sin\phi}{\varepsilon_L}\right) \quad (2)$$

For the upper lobe,

$$\varepsilon_U = \sqrt{\varepsilon^2 + \delta^2 - 2\varepsilon\,\delta\cos\phi} \quad (3)$$

$$\phi_U = sin^{-1}\left(\frac{\varepsilon\ sin\phi}{\varepsilon_U}\right) \quad (4)$$

The film thickness ($h_{L,U}$) in the lower and upper lobes are:

$$h_L = C + d + e_L\,cos\left(\phi - \phi_1 + \theta\right) \quad (5)$$

$$h_U = C + d + e_U\,cos\left(\phi - \phi_2 + \theta\right) \quad (6)$$

The film thickness in dimensionless form is given by $\bar{h} = h_{L,U}/C$.

2.2 Governing equations

The modified Reynolds equation established in this study to determine pressure is consistent with Chen *et. al.*[29] This newly developed equation accounts for the lubricant's non-Newtonian influence and the wall-slip effect on solid-lubricant surfaces of the lemon bearing. The Navier slip boundary condition with mutually perpendicular slip lengths is used to represent the slip boundary conditions on lubricant-sliding surfaces and the non-Newtonian effect is incorporated following the power-law model as $\mu' = m\left(\frac{U}{h}\right)^{n-1}$.[18] where μ' is the amended viscosity, m is the pseudoplastic viscosity constant, U is the velocity of the journal. Since the power-law model is applicable only for shear-thinning liquids ($n < 1$), calculations are applicable and done only for the power-law index (PLI), $n < 1$. The equation to determine the steady-state pressure is given by Eq. (7).

$$\frac{\partial}{\partial x}\left\{\frac{h^3}{12\mu'}\left[\frac{3}{h}\frac{(h+2b_{1x})(h+2b_{2x})}{h+b_{1x}+b_{2x}} - 2\right]\frac{1}{n}\frac{\partial p}{\partial x}\right\} + \frac{\partial}{\partial y}\left\{\frac{h^3}{12\mu'}\left[\frac{3}{h}\frac{(h+2b_{1y})(h+2b_{2y})}{h+b_{1y}+b_{2y}} - 2\right]\frac{\partial p}{\partial y}\right\} = \frac{\partial}{\partial x}\left\{\frac{h}{2}\left[\frac{2u_{1x} + \frac{V_x(h+2b_{1x})}{h+b_{1x}+b_{2x}}}{}\right]\right\} + \frac{\partial}{\partial y}\left\{\frac{h}{2}\left[2v_{1y} + \frac{V_y(h+2b_{1y})}{h+b_{1y}+b_{2y}}\right]\right\} \quad (7)$$

where v_{ix} and v_{iy} are the i^{th} (i = 1, 2) face translational speed along the x and y-direction respectively. V_x and V_y are the velocities of sliding surfaces along the x and y-axis respectively. u_b is the boundary velocity. b_{ix} and b_{iy} are the i^{th} (i = 1, 2) surface slip lengths along the x and y-direction respectively. The dimensionless form of Eq. (7), after omitting the y-velocity component (V_y and v_{1y} as zero), is given by Eq. (8).

$$\frac{\partial^2\bar{P}}{\partial\theta^2}\left\{\frac{\bar{h}^{2+n}}{n}\left[\frac{3}{\bar{h}}\frac{\left(\bar{h}+2B_{1x}\right)\left(\bar{h}+2B_{2x}\right)}{\bar{h}+B_{1x}+B_{2x}} - 2\right]\right\} + \frac{\partial\bar{P}}{\partial\theta}\left\{\frac{\bar{h}^{2+n}}{n}\left[\frac{3(\bar{h}+2B_{1x})}{\bar{h}(\bar{h}+B_{1x}+B_{2x})} - \frac{3(\bar{h}+2B_{1x})(\bar{h}+2B_{2x})}{\bar{h}^2(\bar{h}+B_{1x}+B_{2x})} + \frac{3(\bar{h}+2B_{2x})}{\bar{h}(\bar{h}+B_{1x}+B_{2x})} - \frac{3(\bar{h}+2B_{1x})(\bar{h}+2B_{2x})}{\bar{h}(\bar{h}+B_{1x}+B_{2x})^2}\right]\right\} + \left\{\left(\frac{n+2}{n}\right)\bar{h}^{n+1}\left(\frac{3(\bar{h}+2B_{1x})(\bar{h}+2B_{2x})}{\bar{h}^2(\bar{h}+B_{1x}+B_{2x})} - 2\right)\right\}\frac{\partial\bar{h}}{\partial\theta} + \frac{\partial^2\bar{P}}{\partial\bar{y}^2}\left\{\bar{h}^{2+n}\left(\frac{D}{L}\right)^2\left(\frac{3(\bar{h}+2B_{1y})(\bar{h}+2B_{2y})}{\bar{h}(\bar{h}+B_{1y}+B_{2y})} - 2\right)\right\} = 6\left[\frac{\partial}{\partial\theta}\left\{\frac{\bar{h}(\bar{h}+2B_{2x})}{\bar{h}+B_{1x}+B_{2x}}\right\}\right] \quad (8)$$

where, $\bar{h} = \frac{h}{c}$, $\theta = \frac{x}{R}$, $\bar{y} = \frac{2y}{L}$, $\bar{P} = \frac{pc^{n+1}}{m\omega^n R^{n+1}}$, $\mu' = m\left(\frac{u_b}{h}\right)^{n-1}$. The dimensionless slip-lengths (DSL)

are $B_{1x} = \frac{b_{1x}}{C}, B_{1y} = \frac{b_{1y}}{C}, B_{2x} = \frac{b_{2x}}{C}, B_{2y} = \frac{b_{2y}}{C}$

By Substituting $n = 1$, $b_{1x} = b_{2x} = b_{1y} = b_{2y} = 0$ in Eq. (7), the modified Reynolds equation reduces to the standard Reynolds equation.

2.3 Boundary conditions

According to most scholars, the Reynolds boundary condition is widely recognized in many practical applications,[30–33] and it also provides an intermediate solution that balances precision and complexity. Furthermore, the lubricating film rupture limit and anticipated load-carrying capacity are reasonably precise and well-recognized with this boundary condition. Aside from these considerations, the current study focuses on the dynamic features of lemon bearings at high speeds and light loads, as this is when bearing instabilities are most likely, with cavitation being less visible.[34] Furthermore, in the case of proposed bearings with two lobes and due to the presence of the slip configurations, sub-ambient pressure zones are significantly reduced. As a result, the formulation uses Reynold's boundary conditions (BC) instead of using a mass conservation strategy to deal with challenges like severe cavitation. The pressure BC are:

Pressure is assumed to be zero at the bearing edges. Mathematically,

$$\bar{P} = 0 \; at \; \bar{y} = 0 \text{ and } \bar{y} = 1.0,$$

And, $\bar{P} = 0$ at $\theta = 0$ and $\theta = 2\pi$,

$$\bar{P} = \left(\frac{\partial \bar{P}}{\partial \theta}\right)_{\theta_c<\theta<\theta_s} = 0$$

where (θ_s) and (θ_c) are the start and cavitate points of fluid film.

2.4 Steady state performance analysis

The modified Reynolds equation, Eq. (8), and fluid film domain are discretized using the Finite Difference Method (FDM). Fig. 2 depicts the construction of a finite difference mesh. Solving Eq. (8) for the fluid domain that fulfills the boundary conditions yields the pressure at each node. By satisfying the boundary constraints, a Gauss-Seidel iteration technique with successive over-relaxation (SOR) is employed to achieve the pressure convergence criterion. Converged steady-state pressures are used to evaluate the force components. The assumed attitude angle 'ψ' can be iteratively revised with a minor increment until it converges to 'ϕ' with a tolerance value of 10^{-4}. Simpson's rule is used to calculate load-carrying capacity. Eqs. (9) and (10) represent the forces developed in the lower and upper lobes.

$$\bar{W}_{L,U} = -\int_0^1 \int_0^{2\pi} \bar{P} \cos\theta \; \partial\theta \; \partial\bar{y} \tag{9}$$

$$\bar{W}'_{L,U} = \int_0^1 \int_0^{2\pi} \bar{P} \sin\theta \; \partial\theta \; \partial\bar{y} \tag{10}$$

where, $\bar{P} = \frac{pc^{n+1}}{m\omega^n R^{n+1}}$ is the dimensionless pressure. Using the Eqs. (11) and (12) following Fig. 3, ($\bar{W}_\epsilon$) and ($\bar{W}_\emptyset$) (resulting forces) are resolved.

$$\bar{W}_\varepsilon = \bar{W}_L \cos(\phi - \phi_1) - \bar{W'}_L \cos(\phi + \phi_2) + \bar{W}_U \sin(\phi - \phi_1) - \bar{W'}_U \sin(\phi + \phi_2) \tag{11}$$

$$\bar{W}_\phi = -\bar{W}_L \sin(\phi - \phi_1) - \bar{W'}_L \sin(\phi + \phi_2) + \bar{W}_U \cos(\phi - \phi_1) - \bar{W'}_U \cos(\phi + \phi_2) \tag{12}$$

Resultant dimensionless load,

$$\bar{W} = \sqrt{\bar{W}_\varepsilon^2 + \bar{W}_\phi^2} \tag{13}$$

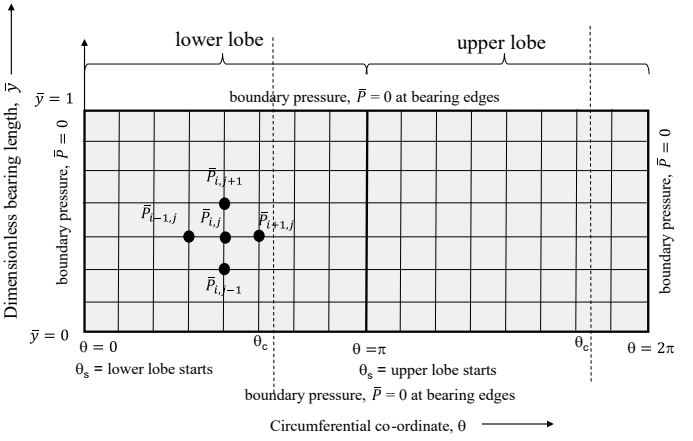

Fig. 2 Discretized Mesh of lemon bearing.

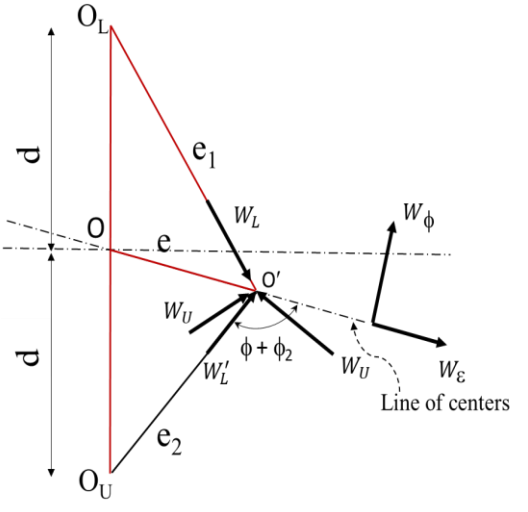

Fig. 3 Resultant forces acting on a lemon bearing.

The attitude angle, side leakage, Sommerfeld number, and friction force are evaluated through the equations Eqs. (14) – (17).

Attitude angle,

$$\phi = tan^{-1}\frac{\bar{W}_\phi}{\bar{W}_\varepsilon} \tag{14}$$

The end-leakage,

$$\bar{Q} = -\int_0^{2\pi}\frac{\bar{h}}{6}\frac{\partial\bar{P}}{\partial\bar{y}}\Big|_{\bar{y}=1} d\theta \tag{15}$$

Sommerfeld number,

$$S = \frac{1}{\pi\bar{W}} \tag{16}$$

Friction force,

$$\bar{F} = \int_0^1\int_{\theta_s}^{\theta_c}\frac{\bar{h}}{2}\frac{\partial\bar{P}}{\partial\theta}d\theta\, d\bar{y} + \int_0^1\int_0^{2\pi}\frac{1}{\bar{h}}d\theta\, d\bar{y} \tag{17}$$

2.5 Stability analysis

Under dynamic conditions, the modified Reynolds equation for pressure distribution in the bearing clearance lubricated with a non-Newtonian lubricant involving wall slip can be expressed as Eq. (18).

$$\frac{\partial}{\partial x}\left\{\frac{h^3}{12\mu'}\left[\frac{3}{h}\frac{(h+2b_{1x})(h+2b_{2x})}{h+b_{1x}+b_{2x}}-2\right]\frac{1}{n}\frac{\partial p}{\partial x}\right\}+\frac{\partial}{\partial y}\left\{\frac{h^3}{12\mu'}\left[\frac{3}{h}\frac{(h+2b_{1y})(h+2b_{2y})}{h+b_{1y}+b_{2y}}-2\right]\frac{\partial p}{\partial y}\right\} = \frac{\partial}{\partial x}\left\{\frac{h}{2}\left[2u_{1x}+\frac{V_x(h+2b_{1x})}{h+b_{1x}+b_{2x}}\right]\right\}+\frac{\partial}{\partial y}\left\{\frac{h}{2}\left[2v_{1y}+\frac{V_y(h+2b_{1y})}{h+b_{1y}+b_{2y}}\right]\right\}-\frac{\partial h}{\partial t} \tag{18}$$

The dimensionless form of Eq. (18) for dynamic analysis after removing the component of surface velocity (along the y-direction, *i.e.*, $v_{1y} = 0$ and $V_y = 0$), is given by Eq. (19).

$$\frac{\partial^2\bar{P}}{\partial\theta^2}\left\{\frac{\bar{h}^{2+n}}{n}\left[\frac{3}{\bar{h}}\frac{(\bar{h}+2B_{1x})(\bar{h}+2B_{2x})}{\bar{h}+B_{1x}+B_{2x}}-2\right]\right\}+\frac{\partial\bar{P}}{\partial\theta}\left\{\frac{\bar{h}^{2+n}}{n}\left[\frac{3(\bar{h}+2B_{1x})}{\bar{h}(\bar{h}+B_{1x}+B_{2x})}-\frac{3(\bar{h}+2B_{1x})(\bar{h}+2B_{2x})}{\bar{h}^2(\bar{h}+B_{1x}+B_{2x})}+\frac{3(\bar{h}+2B_{2x})}{\bar{h}(\bar{h}+B_{1x}+B_{2x})}-\frac{3(\bar{h}+2B_{1x})(\bar{h}+2B_{2x})}{\bar{h}(\bar{h}+B_{1x}+B_{2x})^2}\right]\right\}+\left\{\left(\frac{n+2}{n}\right)\bar{h}^{n+1}\left(\frac{3(\bar{h}+2B_{1x})(\bar{h}+2B_{2x})}{\bar{h}^2(\bar{h}+B_{1x}+B_{2x})}-2\right)\right\}\frac{\partial\bar{h}}{\partial\theta}+\frac{\partial^2\bar{P}}{\partial\bar{y}^2}\left\{\bar{h}^{2+n}\left(\frac{D}{L}\right)^2\left(\frac{3(\bar{h}+2B_{1y})(\bar{h}+2B_{2y})}{\bar{h}(\bar{h}+B_{1y}+B_{2y})}-2\right)\right\} = 6\left[\frac{\partial}{\partial\theta}\left\{\frac{\bar{h}(\bar{h}+2B_{2x})}{\bar{h}+B_{1x}+B_{2x}}\right\}\right]-12\frac{\partial\bar{h}}{\partial\tau} \tag{19}$$

where, dimensionless time $\tau = \omega t$, $u_{1x} = u_b$ (boundary velocity), $V_x = -u_b, V_y = 0, v_{1y} = 0$ and $u_b = R\omega$, (ω-angular velocity of the journal).

2.5.1 Equations of motion

A non-linear time transient analysis is performed for stability analysis utilizing the following equations of motion given by Eqs. (20) and (21). The equations of motion (EOM) along and perpendicular to the line of centers respectively are:

$$\bar{M}\bar{W}_o\left[\ddot{\varepsilon}-\left(\dot{\phi}^2\right)\right] = \overline{W_\varepsilon}+\overline{W_c}\cos\phi \tag{20}$$

$$\bar{M}\bar{W}_o\left[\ddot{\phi}+2\dot{\varepsilon}\left(\dot{\phi}\right)\right] = \overline{W_\phi}-\overline{W_c}\sin\phi \tag{21}$$

Here $\bar{M}$ is the dimensionless mass parameter given as $\bar{M} = \frac{MC\omega^2}{W_o}$, W_o is the Load carrying capacity with the dimensionless load as $\bar{W} = \frac{Wc^{n+1}}{m\omega^n R^{n+2}L}$, for steady and uni-direction load, $\overline{W_c} = \bar{W}_o$ (steady state load = $\bar{W}$).

The first and second-order time derivatives, $\dot{\varepsilon}$ and $\dot{\phi}$ are obtained using the 4RK (fourth-order Runge-Kutta) method for solving the EOM. These time-dependent values are then fed into Eq. (21) to compute $\bar{M}$. A journal center trajectory produced at a specific $\bar{M}$ is used to determine the system's stability and is changed by modifying its value until a trajectory defining the system's marginally stable condition is reached. This continues for various dimensionless mass parameters ($\bar{M}$) values until a critical state is reached in the system below which it is stable, and beyond it which becomes unstable, such $\bar{M}$ values are noted, and a plot of stability is drawn.

3. Validation for the developed model

The present work's generated model is validated by reducing it to a Newtonian fluid ($n = 1$) with a no-slip condition ($B_{ix,iy} = 0$) and comparing the outcomes to the existing literature,[28] as shown in Table 1. The steady-state characteristics are found to be in good agreement in the published literature.

4. Results and discussion

The lemon bearing used in the present study consists of two lobes. The arc length of each lobe is 180 degrees. For analysis, ε ranges from 0.2 to 0.8 with an increment of 0.2. PLI ranges from 0.25 to 0.75 with an increment of 0.25. If PLI = 1, then the lubricant becomes Newtonian. The impact of DSL is explored by varying the DSL from 0.2 to 0.8 on both surfaces of the lemon bearing. The other important parameters set include An ellipticity ratio (δ) of 0.75 and; Aspect ratio (L/D) as unity.

Figure 4a demonstrates the effect of PLI and DSL on dimensionless pressure (DP) at ε = 0.8. Dimensionless pressure increases with an increase in PLI and a decrease in DSL. Lower DSL on the journal surface $B_{1x} = 0.2$ at a higher PLI of 0.75 results in a greater DP of 0.43 when compared to the same lower DSL on the bearing surface $B_{2x} = 0.2$ and

Table 1. Validation of performance characteristics.

Eccentricity ratio, ε	Sommerfeld number, S		Flow rate, Q		Attitude angle, ϕ	
	Pinkus[28]	Present work	Pinkus[28]	Present work	Pinkus[28]	Present work
0.2	0.285	0.27	0.41	0.40	85	84.5
0.4	0.143	0.15	0.41	0.41	80	79.8
0.8	0.060	0.06	0.44	0.43	79	78.2

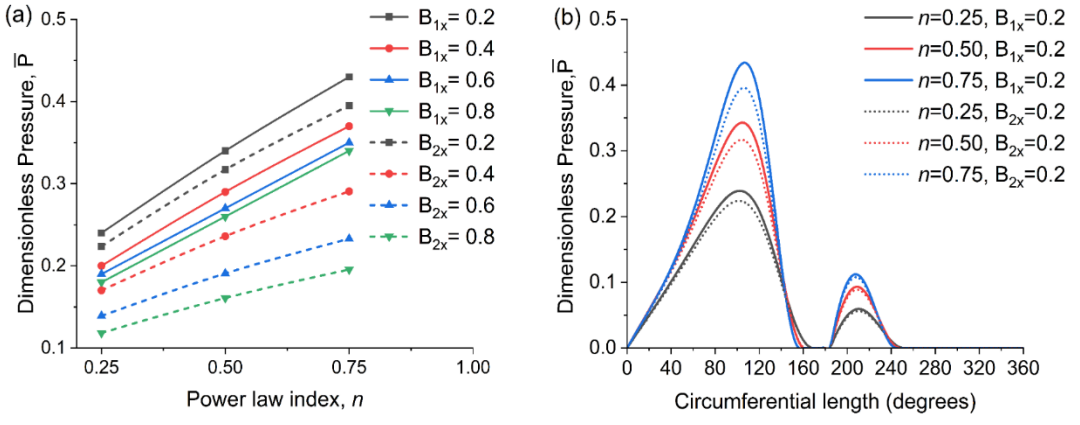

Fig. 4 (a) Influence of PLI on DP for varying DSL on bearing surfaces at ε = 0.8 and (b) variation of DP in lemon bearing for varying PLI with DSL on surfaces.

higher PLI of 0.75, which results in a DP of 0.39. The same pattern of increasing DP with a shorter DSL on the journal surface and a larger PLI is followed even for eccentricity ratios other than 0.8. The DP distribution throughout the circumferential direction at the mid-plane of lemon bearing for varying PLI and DSL on bearing surfaces is shown in Fig. 4b. The DP generated in the lobes of lemon bearing lobes along the circumferential direction in 3D view at B_{1x} = 0.2 and ε = 0.8 is illustrated in Fig. 5.

The variation of S with DSL with varying εas depicted in Fig 6a. The Sommerfeld number decreases as the eccentricity ratio grows for a fixed value of PLI = 0.75. For a given PLI of 0.75, the Sommerfeld number decreases with increasing eccentricity ratio and decreasing DSL for both B_{1x} and B_{2x}. At ε = 0.2, S ranges from 0.28 to 0.54 with DSL on the journal surface, which is less than the variation of S with DSL on the bearing surface, which ranges from 0.41 to 0.75. Fig. 6b reveals the effect of eccentricity ratio on DP for various DSL on the journal surface, B1x. DP is high in all the cases of eccentricity ratio at lower DSL. Maximum DP of 0.43 is developed when B1x = 0.2 and ε = 0.2.

The effect of wall slip and PLI on dimensionless load (NDW) in the lemon bearing can be observed in Fig. 7. DSL is considered on both journal and bearings surfaces for various PLI. Regardless of the surface type, a DSL of 0.2 has a higher load-bearing capability than its successor DSL values within a given set of PLI, viz., 0.25 and 0.75. The load-carrying capacity increases with the increase in PLI and eccentricity

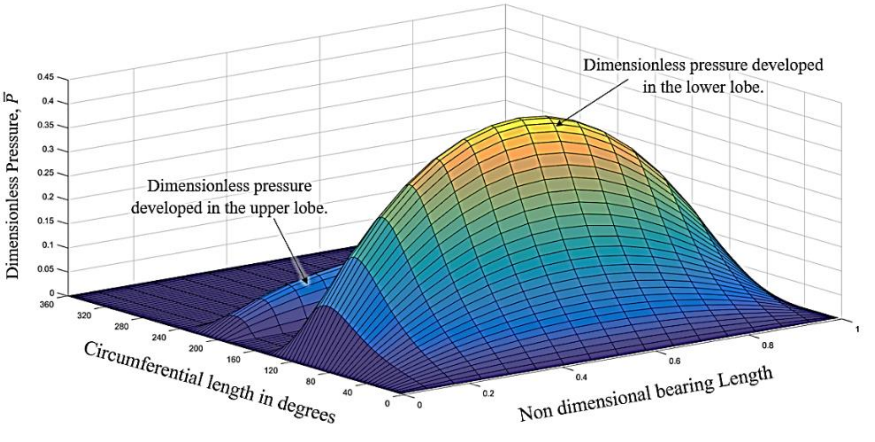

Fig. 5 Pressure profile developed along the circumferential direction of lemon bearing.

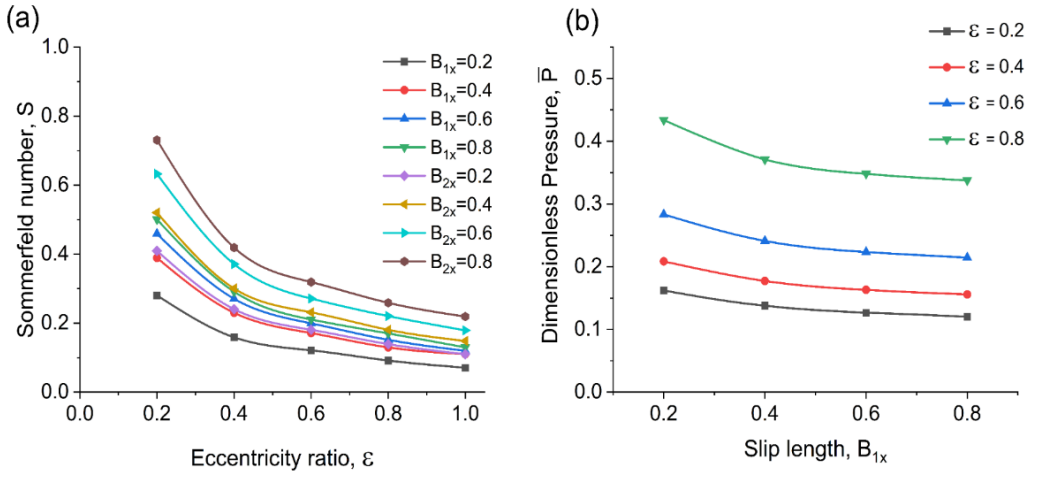

Fig. 6 (a) Influence of DSL on S for varying ε and (b) Influence of DSL on DP for varying ε.

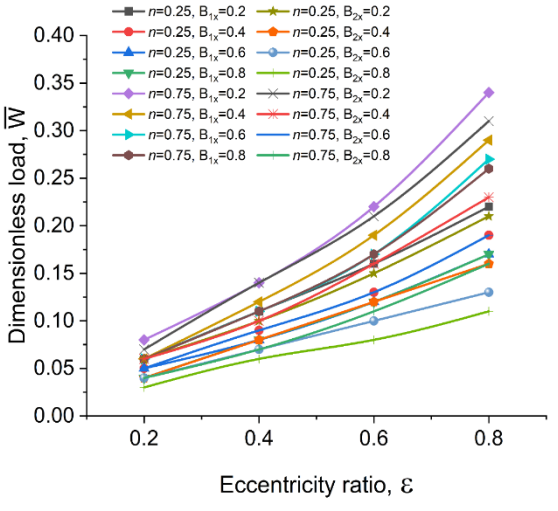

Fig. 7 NDL versus ε for varying DSL on bearing surfaces.

ratio. As a result, it is proved that the load-carrying ability of the lemon bearing with reduced DSL B_{x1} = 0.2 produces higher load-carrying capacity at higher PLI and ε. The highest value of NDW of 0.34 is observed for n = 0.75 with B_{1x} = 0.2 at ε = 0.8. The impact of DSL and PLI on lubricant flow rate for varying ε is shown in Fig. 8a. At a higher eccentricity ratio the displacement of the journal is high, thereby requiring high pressure in clearance leading to higher side leakage. Hence it is observed that the volume flow rate increases with the increase in ε.

The impact of DSL and PLI on friction coefficient for varying ε is depicted in Fig. 8b. When the eccentricity ratio increases, friction increases because the journal moves closer to the bearing surface, diminishing clearance. Friction is found to be less in the case of non-Newtonian fluid in comparison with Newtonian fluid. There is a marginal difference in the friction coefficient when the comparison is made between the non-Newtonian fluids. Larger DSL results in lower friction values because of greater wall slip between the surfaces.

Since exact numerical quantity comparisons are complex, the efficacy of the suggested modified Reynolds equation, methodology, and the most significant outcome of the research

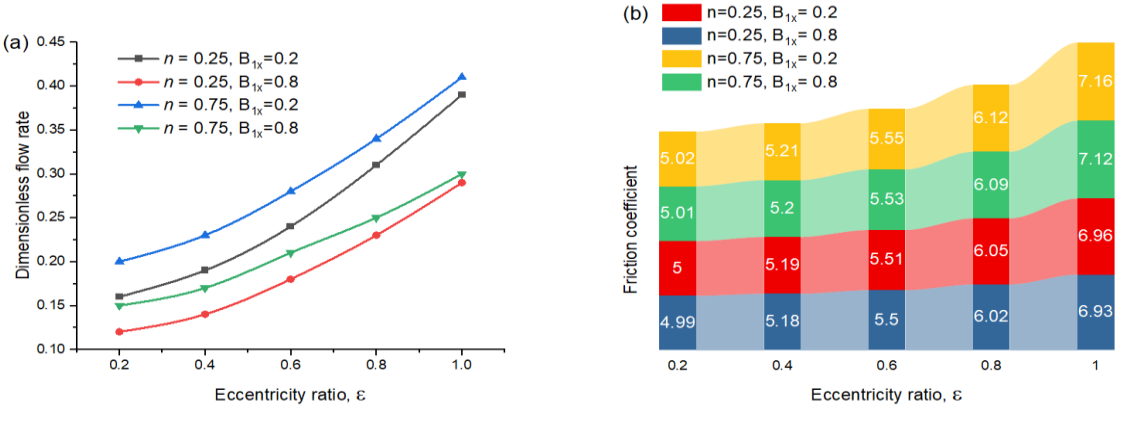

Fig. 8 (a) Influence of DSL and PLI on flow rate for varying ε and (b) Influence of DSL and PLI on friction coefficient for varying ε.

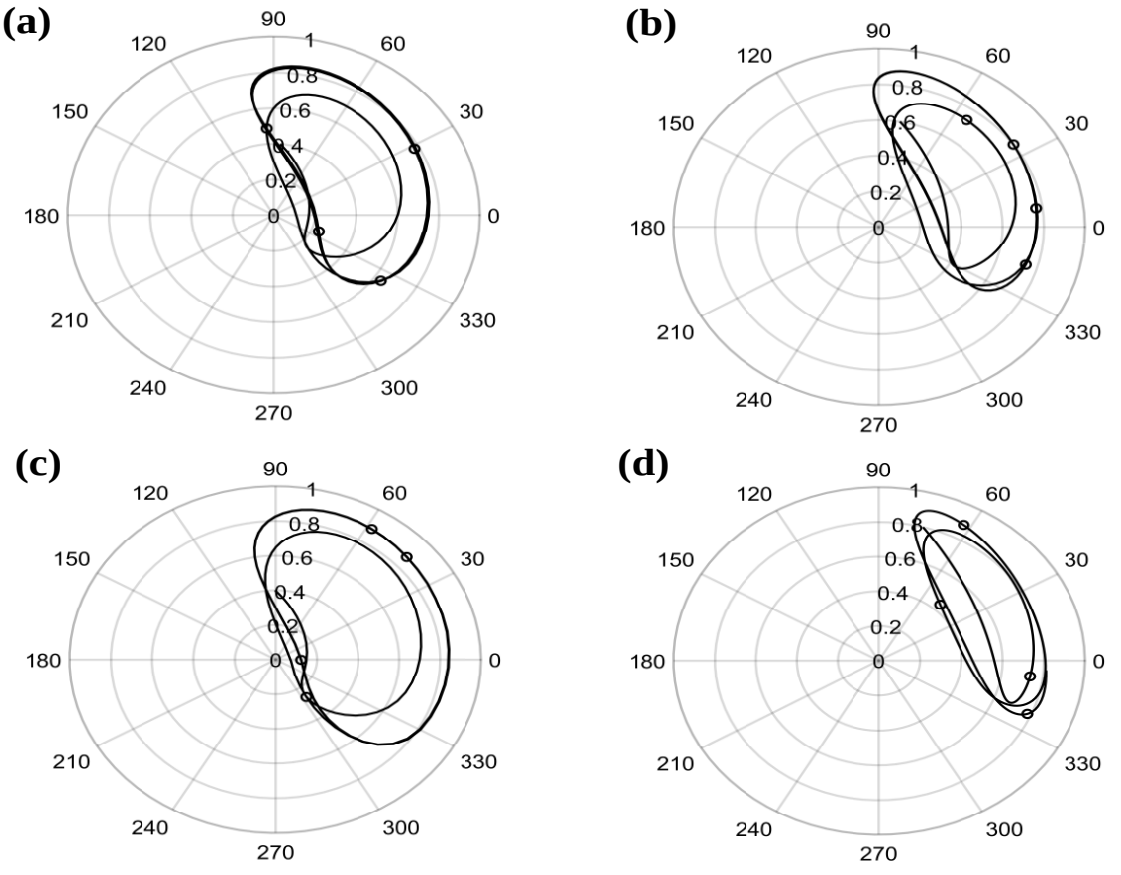

Fig. 9 Journal center trajectory plot (a) n = 0.75, B_{1x} = 0.6, δ = 0.75, ε = 0.4 and $\bar{M}$ = 11.6; (b) n = 0.75, B_{1x} = 0.6, δ = 0.75, ε = 0.6 and $\bar{M}$ = 15.6; (c) n = 0.5, B_{1x} = 0.6, δ = 0.75, ε = 0.4 and $\bar{M}$ = 7.8 and (d) n = 0.5, B_{1x} = 0.6, δ = 0.75, ε = 0.8, $\bar{M}$ = 23.5.

the effort, the inventive proposed model, is compared to prior relevant investigation and their findings[22] in terms of trend comparisons. In the previous relevant existing model, the load-carrying capacity of two-lobe bearings operated with non-Newtonian fluid (n < 1) raised by around 49% compared with the load-carrying capacity of a conventional journal bearing. Whereas the proposed model of lemon bearing, which incorporates the combination of non-Newtonian lubricant and slip length, results in a 59% increase in load-carrying capacity compared to a conventional journal bearing. Overall, the new proposed model's steady-state load-carrying capacity exceeds 10%.

The present study uses non-linear transient analysis to assess the stability of a lemon-bearing accounting slip and non-Newtonian fluid. The non-Newtonian effect is applied by assigning PLI values to less than unity, *i.e.*, for n = 0.25 and 0.75 in steps of 0.25 and by setting an ellipticity ratio of ε = 0.75 throughout the analysis. The DSL is varied in the range 0 to 1 in steps of 0.2.[22] The suggested model can simultaneously find the effect of DSL on both scenarios (B_{1x} or B_{2x}). However, after finding that the lower DSL and larger PLI on the journal surface generated dominating impacts, the analysis discussed here involves only one slip surface (B_{1x}). With everything set, the critical mass parameter for eccentricity ratios varies from 0.2 to 0.8 in steps of 0.2. is evaluated.

To assess the bearing system's stability, the motion of the journal center trajectories plot, which shows the characteristics of the journal center's location, is plotted, and depicted in Figs. 9a-d. These are marginally stable circumstances, where a journal approaches equilibrium by establishing a limit cycle. It can be seen from these journal trajectories that as the PLI increases, so does the mass parameter $\bar{M}$ for a given DSL and eccentricity ratio. The limit cycle moves towards the center of the clearance circle as seen in Fig. 9b at a higher PLI of 0.75 with a $\bar{M}$ = 11.6, indicating better stability in comparison to Fig. 9c with a lower PLI of 0.5 and $\bar{M}$ = 7.8. This concept is very clearer with a comparison of Fig. 9d and Fig. 9a in which the $\bar{M}$ is boosted to 23.5. Another important observation made is by comparing Fig. 9a and Fig. 9b. For a set value of PLI = 0.75, DSL of B_{x1} = 0.6 and δ = 0.75, the mass parameter has raised approximately by 26% with a rise in eccentricity ratio from ε = 0.4 to ε = 0.6. Thus, indicating higher stability being achieved at a higher eccentricity ratio.

To reinforce this fact of higher stability at a higher eccentricity ratio, larger PLI, and lower DSL as described

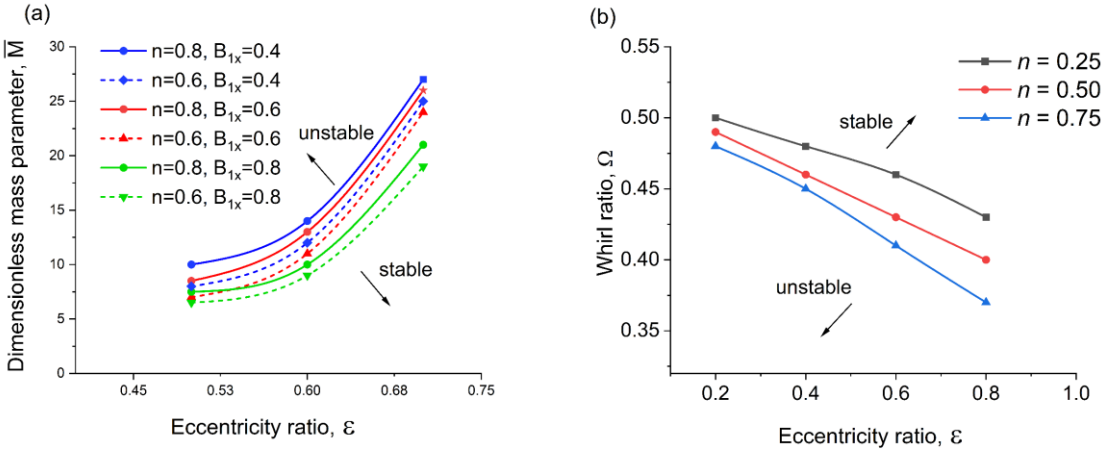

Fig. 10 (a) Dimensional mass parameter versus ε for varying PLI and DSL (b) Whirl ratio variation with ε for varying PLI.

above, a series of stability curves are produced and are presented in Fig. 10a for unevenly selected PLI of 0.6 and 0.8 in association with DSL, B_{1x} = 0.4 to 0.8 and ε = 0.5 to 0.7. It is also clear from the diagram that operating the bearing at a larger eccentricity ratio improves the system's stability. Based on Fig. 10a, it can be shown that the bearing's stability improves with a smaller DSL on the journal surface at greater PLI, but it deteriorates when PLI declines. Operating the bearing at a higher eccentricity ratio enhances the stability of the system. The values of the critical mass parameter at the point when the system becomes marginally stable are obtained at different eccentricity ratios for various values of the power law index with slip B_{1x} = 0.6. The stability curves for the dimensionless mass parameter are shown in Fig. 10b. These curves indicate the influences of PLI on the region of stability. These curves reveal that the lemon bearing is highly stable with a higher PLI of 0.75 at DSL of B_{1x} = 0.6. The stability is found to be increased by 16.21%. The whirl ratio of Lemon bearing reduces with increasing eccentricity ratios and decreasing PLI. For a PLI of 0.75, the lowest whirl ratio is found at an eccentricity ratio of 0.8. This fluctuation is seen for all PLI levels ranging from 0.25 to 0.75. It is also obvious that the bearing should have a greater PLI of 0.75 and a larger eccentricity ratio to operate the Lemon Bearing (LB) with the least amount of whirling.

The variation of $\bar{M}$ with the L/D ratio for different PLI values at B_{1x} = 0.6 is displayed in Fig. 11. The results show that when the L/D ratio is modest, the stability region improves, but as the L/D ratio increases, the stability declines. When L/D = 1 is used, the greatest mass parameter of $\bar{M}$ = 18 is attained, indicating a better stability feature when compared to the stability of the bearing with L/D = 1.5 with $\bar{M}$ = 16. Dimensionless mass parameter provides a particular stable margin for each set of slip length and preload factor for a given L/D ratio. This provides the maximum range of critical mass, beyond which the lemon-bearing system becomes unstable.

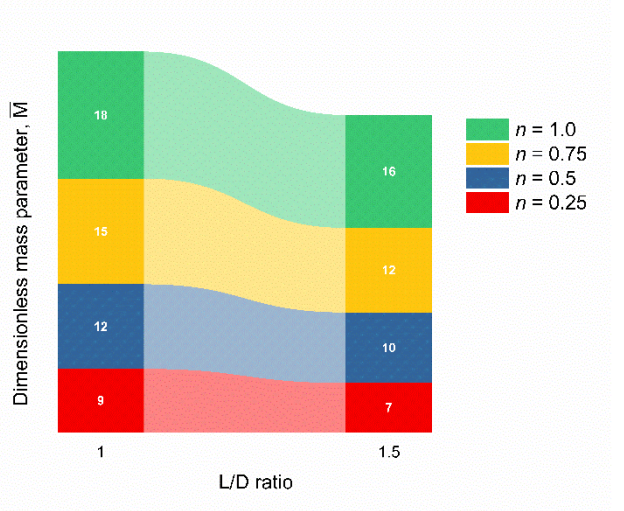

Fig. 11 Variation of $\bar{M}$ with L/D ratio for varying PLI.

5. Conclusions

The effects of the Power Law Index and Dimensionless Slip Length on the static and stability characteristics of the Lemon Bearing are researched in the present work. The steady-state results show that the presence of a wall slip on the journal surface leads to a 10% increase in dimensionless pressure at a higher PLI of 0.75 and a DSL of 0.2. With B_{1x} = 0.2, the bearing's load-carrying capacity is increased by roughly 8% when lubricated with a non-Newtonian lubricant with a higher PLI of 0.75 and a lower DSL. It was found that the friction coefficient is comparatively lower when a wall slip occurs on either of the surfaces when compared to the surface without a wall slip. Furthermore, the flow rate is raised by 6.5% due to pressure rise with an L/D ratio of unity. According to stability analysis, increasing the PLI enhances stability and allows the system to operate in a more stable region. The stability region increases by an average of 19.45% for a given DSL and pre-load factor, where the average is derived using a set of

dimensionless mass parameters acquired at lower and higher PLI values. It can be concluded that for an LB system with a lower SL of 0.2 and a larger PLI of 0.75, the stability is better. In the case of a non-Newtonian fluid with known DSL and PLF, increasing L/D decreases the dimensionless mass parameter, indicating a decrease in the LB system's stability. The whirl ratio of LB decreased as the eccentricity ratio increased, with the lowest whirl ratio for a PLI of 0.75 recorded at an eccentricity ratio of 0.8.

Acknowledgments

The authors would like to thank the Department of Mechanical & Industrial Engineering for facilitating computers to carry out the numerical analysis.

Conflict of Interest

There is no conflict of interest.

Supporting Information

Not applicable.

References

[1] Y. Zhu, S. Granick, Limits of the hydrodynamic no-slip boundary condition, *Physical Review Letters*, 2001, **87**, 1-4, doi: 10.1103/PhysRevLett.87.096105.

[2] Y.Zhu, S. Granick, *Physical Review Letters*, 2002, **88**,106102, doi: 10.1103/physrevlett.88.106102.

[3] Yang, Cho-Yun, Cho-Yu Yang, Cheng-Kuo Sung, Chih-Yung Huang, Design of slip boundary produced by a lotus structure applied to a hydrostatic bearing, *Tribology Letters*, 2014, **55**, 55-64, doi: 10.1007/s11249-014-0331-2.

[4] F. Richard, Salant, Alicia E. Fortier. Numerical analysis of a slider bearing with a heterogeneous slip/no-slip surface, *Tribology Transactions*, 2004, **47**, 328-334, doi: 10.1080/05698190490455348.

[5] F. Aurelian, M. Patrick, H. Mohamed, Wall slip effects in (elasto) hydrodynamic journal bearings, *Tribology International*, 2011, **44**, 868-877, doi: 10.1016/j.triboint.2011.03.003.

[6] C. Wu, Performance of hydrodynamic lubrication journal bearing with a slippage surface, *Industrial Lubrication and Tribology*, 2008, **60**, 293-298, doi: 10.1108/00368790810902232.

[7] G. J. Ma, C. W. Wu, P. Zhou, Wall slip and hydrodynamics of two-dimensional journal bearing, *Tribology International*, 2007, **40**, 1056-1066, doi: 10.1016/j.triboint.2006.10.003.

[8] A. E. Fortier, R. F. Salant, Numerical analysis of a journal bearing with a heterogeneous slip/No-slip surface, *Journal of Tribology*, 2005, **127**, 820-825, doi: 10.1115/1.2033897.

[9] S. Susilowati, M. Tauviqirrahman, J. Jamari, A. P. Bayuseno, Numerical investigation of the combined effects of slip and texture on tribological performance of bearing, *Tribology - Materials, Surfaces & Interfaces*, 2016, **10**, 86-89, doi: 10.1080/17515831.2016.1159781.

[10] T. V. V. L. N. Rao, A. M. A. Rani, T. Nagarajan, F. M. Hashim, Analysis of slider and journal bearing using partially textured slip surface, *Tribology International*, 2012, **56**, 121-128, doi: 10.1016/j.triboint.2012.06.010.

[11] T. V. V. L. N. Rao, A. M. A. Rani, T. Nagarajan, F. M. Hashim, Analysis of micropolar and power law fluid-lubricated slider and journal bearing with partial slip-partial slip texture configuration, *Tribology Transactions*, 2016, **59**, 896-910, doi: 10.1080/10402004.2015.1121310.

[12] L.Qiyin, W. Zhengying, W. Ning ,C. Wei, Industrial Lubrication and Tribology, *Industrial Lubrication and Tribology*, 2015, **67**, 216–226, doi: 10.1108/ILT-05-2013-0055

[13] T. W. Huang, C. I. Weng, C. K. Chen, Analysis of finite width journal bearings with micropolar fluids, *Wear*, 1988, **123**, 1-12, doi: 10.1016/0043-1648(88)90082-8.

[14] M. M. Khonsari, D. E. Brewe, On the performance of finite journal bearings lubricated with micropolar fluids, *Tribology Transactions*, 1989, **32**, 155-160, doi: 10.1080/10402008908981874.

[15] A. Nessil, S. Larbi, H. Belhaneche, M. Malki, Journal bearings lubrication aspect analysis using non-Newtonian fluids, *Advances in Tribology*, 2013, **2013**, 1-9, doi: 10.1155/2013/212568.

[16] Z. S. Safar, Journal bearings operating with non-Newtonian lubricant films, *Wear*, 1979, **53**, 95-100, doi: 10.1016/0043-1648(79)90220-5.

[17] F. Rahmani, R. K. Pandey, J. K. Dutt, Influence of elliptic bore and non-Newtonian rheology of lubricant on the performance and stability of journal bearing, *Procedia Technology*, 2016, **23**, 28-35, doi: 10.1016/j.protcy.2016.03.069.

[18] J. Koravadi, K. Raghunandana, A. M. Chincholkar, Performance characteristics of two-lobe bearings operating with non-Newtonian lubricants, *Journal of Solid Mechanics and Materials Engineering*, 2007, **1**, 421-430, doi: 10.1299/jmmp.1.421.

[19] W. A. Crosby, B. Chetti, The static and dynamic characteristics of a two-lobe journal bearing lubricated with couple-stress fluid, *Tribology Transactions*, 2009, **52**, 262-268, doi: 10.1080/10402000802527773.

[20] K. Raghunandana, B. C. Majumdar, Stability of journal bearing systems using non-Newtonian lubricants: a non-linear transient analysis, *Tribology International*, 1999, **32**, 179-184, doi: 10.1016/s0301-679x(99)00027-4.

[21] S. P. Tayal, R. Sinhasan, D. V. Singh, Finite element analysis of elliptical bearings lubricated by a non-Newtonian fluid, *Wear*, 1982, **80**, 71-81, doi: 10.1016/0043-1648(82)90088-6.

[22] B. J. Das, L. Roy, Analysis and comparison of steady-state performance characteristics of two-axial groove and multilobe hydrodynamic bearings lubricated with non-Newtonian fluids, Proceedings of the Institution of Mechanical Engineers, Part J: *Journal of Engineering Tribology*, 2018, **232**, 1581-1596, doi: 10.1177/1350650118758087.

[23] S. Das, S. K. Guha, A. K. Chattopadhyay, Linear stability analysis of hydrodynamic journal bearings under micropolar lubrication, *Tribology International*, 2005, **38**, 500-507, doi:

10.1016/j.triboint.2004.08.023.
[24] P. B. Kushare, S. C. Sharma, Nonlinear transient stability study of two lobe symmetric hole entry worn hybrid journal bearing operating with non-Newtonian lubricant, *Tribology International*, 2014, **69**, 84-101, doi: 10.1016/j.triboint.2013.08.014.
[25] J. R. Lin, P. J. Li, T. C. Hung, L. J. Liang, Nonlinear stability boundary of journal bearing systems operating with non-Newtonian couple stress fluids, *Tribology International*, 2014, **71**, 114-119, doi: 10.1016/j.triboint.2013.10.010.
[26] B. Chetti, W. A. Crosby, Preload effects on the static characteristics of three-lobe journal bearings lubricated with a couple stress fluid, *Industrial Lubrication and Tribology*, 2019, **71**, 1136-1143, doi: 10.1108/ilt-12-2018-0435.
[27] T. Rao, A. M. A Rani, N. M. Mohamed, H. H. Ya, M. Awang, F. M Hashim, Static and stability analysis of partial slip texture multi-lobe journal bearings, *Proceedings of the Institution of Mechanical Engineers, Part J: Journal of Engineering Tribology*, 2020, **234**, 567-587, doi: 10.1177/1350650119882834.
[28] O. Pinkus, B. Sternlicht, E. Saibel, Theory of hydrodynamic lubrication, *Journal of Applied Mechanics*, 1962, **29**, 221-222, doi: 10.1115/1.3636485.
[29] C. Y. Chen, Q. D. Chen, W. L. Li, Characteristics of journal bearings with anisotropic slip, *Tribology International*, 2013, **61**, 144-155, doi: 10.1016/j.triboint.2012.12.017.
[30] S. Dyk, J. Rendl, M. Byrtus, L. Smolík, Dynamic coefficients and stability analysis of finite-length journal bearings considering approximate analytical solutions of the Reynolds equation, *Tribology International*, 2019, **130**, 229-244, doi: 10.1016/j.triboint.2018.09.011.
[31] T. Snyder, M. Braun, Comparison of Perturbed Reynolds Equation and CFD Models for the Prediction of Dynamic Coefficients of Sliding Bearings, *Lubricants*, 2018, **6**, 1-23, doi: 10.3390/lubricants6010005.
[32] A. Ganesha, P. Raghuvir, S. M. Abdul Khader, Mathematical formulation of the film thickness in a multi-pad externally adjustable hydrodynamic bearing using the transformation technique, *Journal of Computational Methods in Sciences and Engineering*, 2021, **21**, 525-534, doi: 10.3233/jcm-200038.
[33] A. Ganesha, R. Pai, S. Rao, S. A. Khader, Multi-objective optimization and significant analysis of bearing element adjustments on the static performance of an innovative adjustable bearing through design of experiment, *Proceedings of the Institution of Mechanical Engineers, Part J: Journal of Engineering Tribology*, 2021, **235**, 1820-1833, doi: 10.1177/1350650120975240.
[34] A. Bhattacharya, J. K. Dutt, R. K. Pandey, Influence of Hydrodynamic Journal Bearings with Multiple Slip Zones on Rotordynamic Behavior, *Journal of Tribology*, 2017, **139**, 1-11, doi: 10.1115/1.4036629.

Author information

Mr. Amar Murthy A *is an Assistant Professor (Sl. Gr.) in the Department of Mechanical and Industrial Engineering at Manipal Institute of Technology, MAHE, Manipal, India. Tribology, Machine design and Optimization Techniques are the area of his expertise.*

Dr. Raghunandana K *is serving as Professor in the Department of Mechanical and Industrial Engineering at Manipal Institute of Technology, MAHE, Manipal. His areas of interest are Tribology, CAD, Robotics and Composite Materials.*

